抗体は五歳以上の1型糖尿病患者の場合には年齢に関わらず高率に陽性であり、発症早期には八〇%前後で陽性になるが、IA-2抗体の陽性率は年齢によって異なる。小児期発症の1型糖尿病患者では発症早期には七〇～八〇%で陽性となるが、発症年齢が高い患者では陽性率は低く、二六歳以上では発症早期でも二〇%前後とされ、IA-2抗体の測定は一般に若年発症の1型糖尿病の診断に大きな意義がある（図1）[3]。

日本人の一九歳以下で発症した1型糖尿病患者では、GAD抗体に加えて、IA-2抗体を同時に測定することにより一六・四～三〇・九%自己抗体の陽性率が上昇し、診断感度が向上する[4]。なお、GAD抗体同様、罹病期間とともに抗体価、陽性率とも低下するので、発症から長期間を経過した患者では、膵島関連自己抗体が陰性でも、1型糖尿病（1A）を否定できない。

図1 年齢別にみた1型糖尿病におけるIA-2抗体とGAD抗体の陽性率

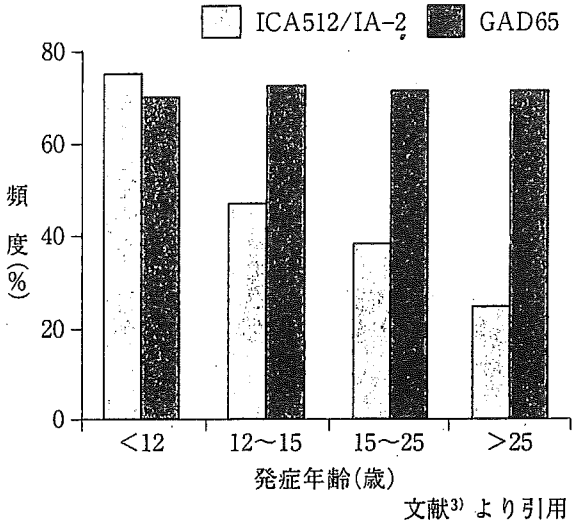

文献[3]より引用

IA-2抗体は、緩徐進行1型糖尿病（slowly progressive IDDM；SPIDDM）の指標としての価値は、ICAやGAD抗体に劣る。SPIDDMではIA-2抗体は一般にGAD抗体陽性例にしか認められないので、IA-2抗体を調べても診断感度は高くならない。しかし、GAD抗体陽性のNIDDMの中で、IA-2抗体陽性例はインスリン依存へ進行しやすいので、IA-2抗体の測定はインスリン依存への進行を予知する上で、特異性を高めることに貢献する[5]。なお、SPIDDMでIA-2抗体の陽性率が低いのは発症年齢を反映していると考えられる。

IA-2抗体は1型糖尿病発症予知の指標としても有用であり、欧米では1型糖尿病患者の近親者に対し、IA-2抗体を測定することによって発症を予知し、予防を企図する研究が盛んに行われている。

以上のように、IA-2抗体は1型糖尿病の診断や発症予知に有用であるが、健康保険の適用は以下のようである。すなわち、「抗IA-2抗体精密測定は、糖尿病の診断が確定し、かつ、GAD抗体陰性が確認された三〇歳未満の患者に対し、インスリン依存型糖尿病（IDDM）の診断に用いた場合に算定する。なお、糖尿病の診断が確定し、かつ、GAD抗体陰性が確認された三〇歳以上の患者に対しては、診療報酬明細書の摘要欄にその理由および医学的根拠を詳細に記載すること」とされる。SPIDDMの進行予知の指標や1型糖尿病の発症予知の指標としては認められていない。

（埼玉社会保険・病院内科部長　丸山太郎）

〔文　献〕

1）丸山太郎：診断と治療 91(9)：1533, 2003.
2）丸山太郎：内分泌・糖尿病科 20(5)：452, 2005.
3）Kasuga A, Ozawa Y, Maruyama T, et al：Endocr J 44(4)：485, 1997.
4）松浦信夫，内潟安子，浦上達彦，他：プラクティス 16(5)：567, 1999.
5）Kasuga A, Ozawa Y, Maruyama T, et al：Diabetes Care 20：679, 1997.

進行膵癌のゲムシタビンによる治療

Q 進行膵癌の治療について以下を。

一、ゲムシタビン単独投与の成績。

二、ゲムシタビンと他の抗癌剤との併用療法の効果。

三、放射線療法の有効性。

（岡山県　T）

A 一、ゲムシタビン単独投与の成績

ゲムシタビンはピリミジン骨格を有する代謝拮抗剤であり、細胞内において三リン酸化物に代謝され、DNAの合成を阻害する。しかもゲムシタビンは腫瘍への蓄積効果が高いことが示されている。

Burrisら[1]により、進行膵癌の化学療法において、ゲムシタビンは従来の標準選択薬の5-FUとの無作為比較試験で、奏効率は五・四%と低率であったが症状緩和効果が二三・八%と有意に高率で、五〇%生存期間（MST）も五・七カ月と有意に優れていた。

筆者ら[2]は多施設共同研究で、進行膵癌四九症例に初回化学療法としてゲムシタビンを投与し、その治療効果、有害事象を検討した。腫瘍縮小効果は、partial response（PR）五例（一〇%）で、stable disease（SD）一二五例（五一%）、progressive disease（PD）一六例（三二・七%）、判定不能三例（六%）でそれほど顕著ではなかった。四九例のMSTは一八一日、一年生存率は一四・三%であったが、癌性胸腹水を有する群は胸腹水のない群に比し有意な短縮を認めた。QOLが保たれ、外来治療が可能であった。

有害事象については一般的な抗腫瘍薬と大きな差異はない。多施設四九例の検討では、軽度の骨髄抑制はほとんどの症例で生じると考えてよいが、NCI-CTC gradeにおけるgrade 3以上の骨髄抑制は白血球減少一四%、好中球減少二二%、血小板減少七%、ヘモグロビン減少三%と、それほど高頻度ではなかった。その三分の二は一コース目に生じていた。非血液学的有害事象としてはgrade 3の悪心・嘔吐を五%に認めたが、その他はgrade 1～2の発熱、皮疹、疲労、食欲低下が主なものであった。

発熱は投与直後の他に、数日後に生じることもある。皮疹は投与開始早期に瘙痒感を伴わないか、あってもきわめて軽度であり、投与を継続していると軽快する場合が多いと思われるが、高度の皮疹でゲムシタビンの投与を断念せざるをえない症例もある。長期に投与する場合は間質性肺炎、hemolytic uremic syndrome（HUS）や浮腫、肺水腫、心嚢液貯留などが生じる場合があるので注意を要し、投与量や投与方法の工夫が必要である。

以上のように、ゲムシタビンによる腫瘍縮小効果は軽度であるが、症状緩和効果を認め、外来でも安全に投与できることから、進行膵癌の化学療法の第一選択薬である。

二、他の抗癌剤との併用効果

ゲムシタビンの治療効果を高めるために、ゲムシタビンをベースとした併用化学療法も種々のphase III study（表1）が試みられている。また、分子標的治療薬のうちMMP阻害剤（marimastat）と、膵癌には高率にK-rasの突然変異がみられることにより注目されたras蛋白の機能発現に必要なfar-

表1　主な海外第III相臨床試験成績

報告者/文献	薬剤	投与量（mg/m²）	症例数	MST	1年生存率（%）	PFS	奏効率（%）
Berlin JD：JCO, 2002	gemcitabine	1,000	162	5.4カ月	＜20	2.2カ月	5.6
	gemcitabine 5-FU（bolus）	1,000 600	160	6.7カ月	＜20	3.4カ月	6.9
Colucci G：Cancer, 2002	gemcitabine	1,000	54	20週	11	8週	9.2
	gemcitabine CDDP	1,000 25	53	30週	11.3	20週	26.4
Rocha Lima CMS：JCO, 2004	gemcitabine	1,000	169	6.6カ月	22	3.0カ月	4.4
	gemcitabine CPT-11	1,000 100	173	6.3カ月	21	3.5カ月	16.1
Louvet C：JCO, 2005	gemcitabine	1,000	156	7.1カ月	27.8	3.7カ月	17.3
	gemcitabine oxaliplatin	1,000 100	157	9カ月	34.7	5.8カ月	26.8

MST；median survival time
PFS；progression free survival

nesyltransferase inhibitorであるR115777とは、それぞれゲムシタビン単独および併用との比較試験でもMSTは同程度であった。すなわち、ゲムシタビンとの併用療法は腫瘍縮小率を向上させるものの、生存期間延長には寄与しない結果である。

最近、ゲムシタビンとシスプラチン、エピルビシン、5-FUとの併用療法（PEFG療法）やエルロチニブとの併用療法ではゲムシタビン単独療法に比べ、生存期間を有意に延長したことが報告されたが、いずれの報告もその差はわずかであり、また併用群での有害事象発生頻度は高率であった。

三、局所進行膵癌の放射線療法

これまでの放射線化学療法は、5-FUを増感剤として週五日静注または持続点滴静注（二〇〇mg/m²/日）を行い、X線照射は一日に一・八Gy、二八日間で五〇・四Gyとし、照射後は一～二週おいて維持化学療法として週一回5-FU点滴（五〇〇mg/m²）が一般的であった。最近は、放射線増感剤でもあるゲムシタビンを用いての放射線化学療法について、各地で精力的に検討されている。

本邦ではIkedaら[3]が、トータル五〇・四Gyとゲムシタビン二五〇mg/m²を推奨容量とし、四〇%のPR例を報告している。その他、照射線量五〇・四Gyに対し、低用量ゲムシタビン四〇mg/m²週二回投与の報告、ゲムシタビンの投与量を通常量の一〇〇〇mg/m²用い、放射線照射量を三六Gyでの報告等であるが、強い副作用出現が問題点である。

従来の5-FU増感剤に比べ、投与ゲムシタビン量の問題等、今後の課題も多いが、維持化学療法剤としてはゲムシタビンがより延命効果に寄与すると思われる。いずれにしても、現時点では遠隔転移を認めない手術不能の進行膵癌に対し、放射線化学療法は延命効果の面から有力な治療法と考える。

（国立病院機構九州がんセンター消化器内科医長　船越顕博）

〔文　献〕

1) Burris III HA, Moore MJ, Andersen J, et al : J Clin Oncol 15 : 2403, 1997.
2) 澄井俊彦，松尾　享，井口東郎，他：膵臓 19：479, 2004.
3) Ikeda M, Okada S, Tokuuye K, et al : Br J Cancer 86 : 1551, 2002.

内臓脂肪の生活習慣病との関係およびその簡便な測定法

Q

二〇〇五年四月、メタボリックシンドロームの診断基準が示された。腹囲の増加、すなわち内臓脂肪の蓄積が将来の生活習慣病発生に関与するとのことであるが、左記を。

一、内臓脂肪はどのような機序によってそれぞれの生活習慣病を引き起こすのか。蓄積されるのは同じ中性脂肪と理解しているが、皮下脂肪との代謝機能の差異について。

二、内臓脂肪の計測法として、腹囲、エコー、CTなどの他に検診時に使用できる簡便な方法があれば。

（秋田県　S）

A

一、内臓脂肪の生活習慣病との関係

内臓脂肪の蓄積は高脂血症、糖尿病、高血圧を合併し、動脈硬化性心血管疾患と密接に関連し[1]、メタボリックシンドロームの診断基準で必須項目となっている[2]。内臓脂肪の蓄積は門脈血中の遊離脂肪酸、グリセロールを増加させ、それらが直接肝臓に流入することにより代謝異常を引き起こす。また、脂肪組織、特に内臓脂肪はさまざまなアディポサイトカインを分泌し、脂肪細胞の機能異常が合併症を引き起こすことが明らかとなっている（図1）。

脂質代謝異常に関しては、増加した門脈血中の遊離脂肪酸が肝臓に流入し、超低比重リポ蛋白（VLDL）の合成を促進し、高トリグリセリド血症を、リポ蛋白リパーゼの低下により低HDL血症を来す。

耐糖能異常に関しては肝臓内に流入した遊離脂肪酸、グリセロールがインスリン抵抗性を来すこと、抗糖尿病作用を有するアディポネクチンの減少、糖尿病を促進する腫瘍壊死因子α（TNF-α）の増加が耐糖能異常を引き起こす。高血圧に関してはアディポネクチンの低下、アンジオテンシノーゲンの増加などが考えられている。

動脈硬化に関しては高脂血症、耐糖能異常、高血圧の他、抗動脈硬化作用を有するアディポネクチンの減少、動脈硬化を促進するプラスミノゲン活性化阻止因子1（PAI-1）の増加というアディポサイトカインの分泌異常が直接動脈硬化に結びつく。

内臓脂肪と皮下脂肪との代謝機能の差違については、ご指摘のよ

ORIGINAL ARTICLE

Radiation Medicine: Vol. 23 No. 5, 364–370 p.p., 2005

Quantitative Tissue Blood Flow Evaluation of Pancreatic Tumor: Comparison between Xenon CT Technique and Perfusion CT Technique Based on Deconvolution Analysis

Hisashi Abe,[1] Takamichi Murakami,[1] Masaru Kubota,[2] Tonsok Kim,[1] Masatoshi Hori,[1] Masayuki Kudo,[3] Kazuhiko Hashimoto,[2] Shoji Nakamori,[2] Keizo Dono,[2] Kaname Tomoda,[1] Morito Monden,[2] and Hironobu Nakamura[1]

Purpose: There has been one report that tissue blood flow (TBF) quantification with xenon CT was effective in predicting the therapeutic response to an anticancer drug in pancreatic cancer. The purpose of this study was to evaluate the correlation between the TBF of pancreatic tumors calculated with xenon CT and those with perfusion CT, in order to evaluate whether perfusion CT could replace xenon CT.

Materials and Methods: Nine patients with pathologically proved pancreatic tumors who underwent both xenon CT and perfusion CT were included.

Results: Quantitative TBF of pancreatic tumors measured by perfusion CT ranged from 22.1 to 196.2 ml/min/100 g (mean±SD, 52.6±54.8 ml/min/100 g). In contrast, those obtained by xenon CT ranged from 10.3 to 173.6 ml/min/100 g (mean±SD, 47.4±49.4 ml/min/100 g). There was a good linear correlation between xenon CT and perfusion CT ($y=0.8537x+2.48$, $R2=0.895$: $p<0.05$).

Conclusion: The TBF of pancreatic tumors measured by xenon CT and perfusion CT techniques showed a close linear correlation. We can expect that perfusion CT based on the deconvolution algorithm may replace xenon CT to predict the effect of pancreatic tumor treatment with anticancer drugs.

Key words: perfusion CT, xenon CT, pancreatic tumor

Introduction

Pancreatic cancer is the fourth leading cause of cancer death in Western countries.[1] Therapeutic methods for pancreatic cancer include operation, chemotherapy, and radiation. Although surgical resection is the most effective method, sometimes it is not possible in advanced cases because of the difficulty of early detection, invasive growth, and metastases to liver and lymph nodes even if tumor size is small.[2] In such cases, chemotherapy with an anticancer drug should be used, although some cases unfortunately have only side effects without tumor reduction from chemotherapy. Recently, a new anticancer drug, GEMZAR® (gemcitabine HCl for injection) (Gemzar, Eli Lilly and Company, IN, USA), has been introduced and is expected to improve the prognosis of pancreatic cancer.[3-5] However, as in the case of many anticancer drugs, GEMZAR® (gemcitabine HCl for injection) is not always effective for all pancreatic cancers. In some cases, the drug is amazingly effective; on the other hand, in other cases it is not effective, but even harmful, because of severe side effects. The reason for this difference is unclear, however, it is essential for patients to know whether the drug will be effective or not, because, if prediction were possible, patients would be able to avoid ineffective anticancer drug therapy with severe side effects. This would dramatically lower the cost of medical care as well. In order to avoid ineffective chemotherapy, some have tried to predict therapeutic effect with radiological imaging such as MR spectroscopy, FDG-PET, and perfusion CT, and some good results have been reported.[6-9]

Received October 28, 2004; revision accepted February 23, 2005.

Departments of [1]Radiology and [2]Surgery and Clinical Oncology, Osaka University Graduate School of Medicine

[3]Imaging Application Technical Center, GE Healthcare

Reprint requests to Takamichi Murakami, M.D., PhD., Department of Radiology, Osaka University Graduate School of Medicine, 2-2 Yamadaoka, Suita, Osaka 565-0871, JAPAN.

Among these reports, one author described that it was useful to evaluate the TBF of pancreatic adenocarcinoma for chemotherapeutic response with xenon CT.[9] However, xenon CT requires special equipment. Recently, some reports[10-13] have indicated the ability of perfusion CT to evaluate TBF. We hypothesized that, if a good correlation in TBF exists between xenon CT and perfusion CT, we could replace xenon CT with perfusion CT for prediction of the response to GEMZAR® in pancreatic cancer.

The purpose of this study was to evaluate the correlation between the calculated TBF of pancreatic tumors with xenon CT and those with perfusion CT based on a deconvolution algorithm.

Materials and Methods

Patients

Nine patients with pathologically proved pancreatic tumors, who underwent both xenon CT and perfusion CT, were included in this study. Eight patients had pancreatic adenocarcinoma, and one had islet cell tumor. Four were males and five females, and their age range was between 29 and 80 years (mean, 65 years). Tumor size was between 2.5 cm and 5 cm in diameter (mean, 3.7 cm). The intervals between the two procedures were as follows: the same series in five cases, three days in one case, one week in one case, two weeks in one case, and three months in one case. All patients had given their informed consent to be included in the study, which was conducted in accordance with the principles of the Declaration of Helsinki.[14]

Xenon CT technique

The xenon CT technique was used to assess regional TBF by using the wash-in/wash-out protocol, which has been previously used for measurement of regional cerebral blood flow.[15] The Kety-Schmidt equation, based on the Fick principle used for cerebral blood flow evaluation, was also used.[16,17] Xenon gas (XENON COLD®, Anzai Medical Co., Ltd., Tokyo, Japan) was used as the nonradioactive xenon gas, and the xenon gas inhalation system with a closed gas circuit (AZ-725, Anzai Medical Co., Ltd.) was used. The xenon concentration in the respiratory circuit (end-tidal peak xenon values) was continuously measured during examination by a xenon monitor incorporated in the AZ-725 circuit. End-tidal peak xenon values were recognized automatically and fitted to a monoexponential curve (end-tidal xenon curve).[18] Changes in arterial blood xenon concentrations were estimated based on the end-tidal xenon curve.[19]

Changes in CT values of the pancreatic tumor were measured by a helical CT (LightSpeed Ultra, GE Healthcare, WI, USA). Following identification of the pancreatic tumor by precontrast CT scan, four axial images with a 10-mm slice thickness and including the pancreatic tumor were obtained incrementally as baseline CT images prior to xenon inhalation. In the next step, the patient inhaled 25% (vol/vol) xenon gas for 4 minutes (wash-in), followed by breathing room air for 5 minutes (wash-out).[15] In the meantime, CT scans were acquired at each level at one-minute intervals. As many as ten CT images per patient were obtained in total, including the baseline image at each level. Exposure factors were 100 kVp, 200 mA, and 1-second scans, and patients were required to hold their breath for 7 seconds during a series of scans at 4 levels. Smoothing with a 9×9 pixel filter was used to reduce noise on the CT images. Body movement related to respiration was taken into account, and changes in pancreatic position on each enhanced CT image were digitally corrected relative to the baseline image on the screen of a blood flow imaging analysis computer system (AZ-7000W, Anzai Medical Co., Ltd.).

The AZ-7000W was also used to create color maps for TBF from images obtained by xenon CT as well as confidence images, which showed the variance in value for each pixel based on the least-square method. High TBF appeared as red regions, and low TBF as blue regions. The confidence images were used to evaluate the reliability of the TBF value for each pixel of the image.[20,21] TBF was determined by placing regions of interest (ROI) on the pancreatic tumor on the color maps. When the ROI of the tumor was small, we carefully placed small ROI on the small tumor (Fig. 1B).

Perfusion CT technique

The basic theory of deconvolution analysis was reported by Meier and Zierler in 1954.[22] Tissue contains many arteries and veins, and numerous capillary vessels. These form a very complex blood-supply system. However, based on the central volume principle, one simple equation is derived, that is, TBF (ml/100 g/min) = TBV (tissue blood volume, ml/100 g)/MTT (mean transit time, min). MTT is the average time that blood passes through a capillary network with various lengths in a target tissue. When iodinated contrast material can be considered as a purely intravascular tracer, during the bolus passage of contrast material in tissue, and concentration of the contrast material within tissue, Q(t) with dynamic CT. In minute scales, contrast material injected as a bolus for a very short time will fill the entire capillary network in tissue and arrive at equilibrium, and then wash-out from the network. The graph of this is called the impulse residue function, R(t). As Meier and Zierler described,

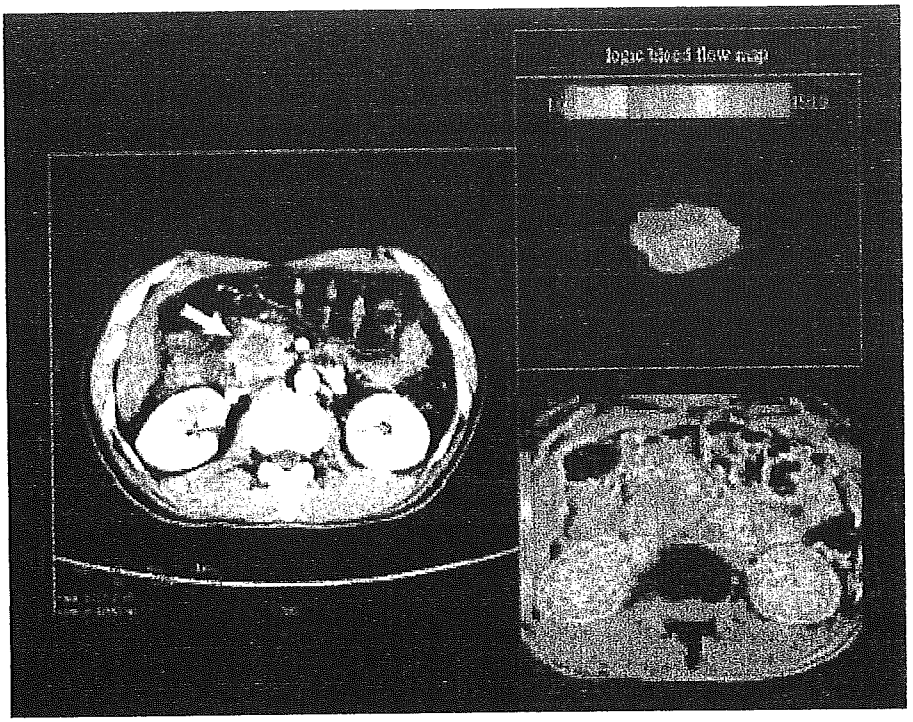

Fig. 1. A 42-year-old man with pancreatic head cancer.
The CT image (A) shows a pancreatic head tumor (*arrow*) that appears on both xenon CT (B) (TBF=26.0 ml/mg/100 g) and perfusion CT (C) (TBF=33.3 ml/mg/100 g) images.

if contrast material volume is linear with respect to the arterial input and F is constant in time, the next equation comprises:

$$Q(t)=F \cdot Ca(t)*R(t)$$

where * is the convolution operator. We know Q(t) and Ca(t) with dynamic CT, so using opposite convolution (called as deconvolution), we can calculate F · R(t). The height of F · R(t) is TBF, and the area under F · R(t) is TBV. MTT can be calculated with the equation MTT=TBV/TBF.[23] However these equations should be applied only in tissues such as brain, in which intravascular tracer never permeates into extravascular space because of the blood brain barrier. While in tissue such as pancreas, intravascular tracer easily permeates into extravascular space, so a correction equation for permeability must be applied to measure TBF correctly. In tissue with permeability, its R(t) shape changes to a broad-based graph, because contrast material in extravascular space returns to vessels gradually and slowly even after the passing of intravascular contrast material. If the proportion of the contrast material that permeates into extravascular space is represented as E, R(t) for contrast material of intravascular space is (1−E)·Ri(t), and R(t) for contrast material permeated into extravascular space is represented as E · Re(t). As a result, in tissue with the permeability, TBF is calculated with an equation: R(t)=(1−E) · Ri(t)+E · Re(t).

We used a helical CT unit (LightSpeed Ultra, GE Healthcare, WI, USA) to measure the TBF of pancreatic tumors with perfusion CT. The scanning position for perfusion CT was decided by using precontrast CT of the upper abdomen for patients with pancreatic tumor. Two slices of 10 mm in thickness, which were positioned at the center of a tumor, were selected and fixed. A bolus infusion of 0.5 ml/kg/ml of 300 mg/ml iodine concentration contrast material (Omnipaque, Daiichi Pharmaceutical Co., Ltd., Tokyo) at a rate of 5 ml/s was given via a 20-gauge intravenous catheter using an automatic injector. Eight seconds after the initiation of contrast material injection, CT scanning started. During 40 continuous seconds of breath hold, data were collected. The parameters of perfusion CT were 120 kVp, 60 mAs. All CT data were analyzed by an imaging workstation (Advantage Workstation 4.0, GE Healthcare, WI, USA) with commercial software (CT perfusion 3, GE Healthcare). The software uses the deconvolution algorithm as a measurement principle.[10,11,24] This software is developed with capillary permeability in consideration, as reported by Johnson *et al.*,[25] so the algorithm of this software is different from the software used in brain CT perfusion study. Tumor TBF was determined by placing the ROI in the same way as in xenon CT (Fig. 1C).

Table 1. Values of tissue blood flow measured by xenon CT and perfusion CT

Case	Pathology	Perfusion CT	Xenon CT
1	Adenocarcinoma	43.4	26.3
2	Adenocarcinoma	23.1	10.3
3	Gastrinoma	196.2	173.6
4	Adenocarcinoma	50.0	19.7
5	Adenocarcinoma	36.1	54.2
6	Adenocarcinoma	33.3	26.0
7	Adenocarcinoma	22.1	45.4
8	Adenocarcinoma	45.0	46.9
9	Adenocarcinoma	24.4	24.3
			ml/mg/100 g

Statistical analysis

Differences in TBF between xenon CT and perfusion CT were analyzed using regression analysis. A p-value of less than 0.05 was considered statistically significant.

Results

The quantitative TBF of pancreatic tumors measured by perfusion CT ranged from 22.1 to 196.2 ml/min/100 g (mean±SD, 52.6±54.8 ml/min/100 g). In contrast, those obtained by xenon CT ranged from 10.3 to 173.6 ml/min/100 g (mean±SD, 47.4±49.4 ml/min/100 g). A comparison of the quantitative values obtained by xenon CT and perfusion CT in each pancreatic tumor is shown in Table 1. There was a good linear correlation between xenon CT and perfusion CT (y=0.8537x+2.48, R2=0.895: p<0.05) (Fig. 2).

In analysis of eight adenocarcinoma cases, the correlation between xenon CT and perfusion CT was as follows; y=0.14x+26.7, R2=0.01: p<0.05.

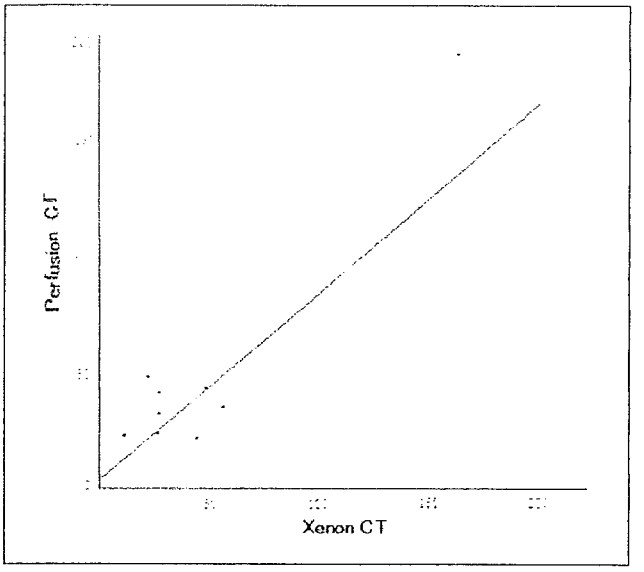

Fig. 2. All quantitative values are plotted on this graph. A very good linear correlation is shown (y=0.8537x+2.48, R2=0.895, p<0.05).

Discussion

Many studies of the quantitative measurement of TBF have been reported, especially those on brain blood perfusion, and are based on various methods such as PET, SPECT, perfusion MRI, xenon CT, and perfusion CT.[12,18,26,27] Among these methods, the nuclear medicine approach has the longest history and is regarded as the gold standard for cerebral blood flow.[26] The weak point of this method is that nuclear medicine approaches such as PET and SPECT require radioisotopes and special equipments, which are very expensive. Moreover, the spatial resolution of their imaging modalities are much inferior to that of CT. MRI also can be used for TBF. However, it is hard to calculate TBF quantitatively, because the signal enhancement of non-specific MR contrast medium, which is a gadolinium complex, does not show a linear correlation to the concentration of contrast medium and influences the signal intensity of vessels and tissues around vessels. CT provides much clearer and sharper images than other modalities, and we can evaluate color maps of quantitative TBF and clear anatomical images with CT at the same time. In addition, CT is the most practical and universal machine on clinical site and is used frequently for the abdominal area. One report recently described a good correlation between cerebral blood flow measured by perfusion CT and ^{15}O-PET, which is the gold standard of reference for cerebral blood flow.[12] In non-CNS parts, Faria *et al.* reported good correlation between blood flow measurements obtained from ^{15}O-PET and perfusion CT at low and moderate flows.[27] Based on these reports, we hypothesized that perfusion CT would be able to measure quantitative TBF in pancreas as well.

There are two methods available to calculate TBF with CT namely, xenon CT and perfusion CT. The history of xenon CT has about 30 years,[28] whereas perfusion CT was first described by Miles in 1991.[29] Regardless of how long their history, there have been only a few reports on quantitative pancreatic blood flow measured by CT.[30,31] The scanning time, during which patients had to hold their breath, was too long for patients to maintain the same position, although same position must be held in order to calculate TBF precisely. However, recent technical innovations of CT, such as fast imaging, have overcome the problem by reducing breath-holding duration.

Kubota *et al.* reported that TBF measured by xenon CT might predict the response of pancreatic cancer to anticancer drugs.[9] In their article, they noticed that, in pancreatic cancer with higher TBF, chemoradiation therapy decreased the tumor marker, and prognosis was better than that of cancer with lower TBF; thus they concluded that the evaluation of TBF with xenon CT in pancreatic cancer would be useful to predict the therapeutic effect of chemoradiation therapy. To our knowledge, their report is the first to describe the possibility of predicting treatment with an anticancer drug in pancreatic cancer. In this report, they used xenon CT to calculate TBF, which was used to assess regional TBF by using the wash-in/wash-out protocol and has been previously used for the measurement of cerebral blood flow. However, we thought that xenon CT might not be practical, because xenon CT requires special materials, such as xenon gas and specialized equipment, and the procedure for calculating TBF is complicated.

Compared with the complexity of xenon CT, perfusion CT needs only universally available materials to measure blood flow, such as iodine contrast material and a workstation, although CT perfusion software is required. Moreover, perfusion CT can be performed in the same clinical session, just before usual dynamic CT with iodine contrast medium.

In the procedure of perfusion CT, the past method using the Fick principle requires a very high injection rate of contrast material via a peripheral vein, such as 10-20 ml/s, rendering it very dangerous in patients with fragile or thin vessels. However, the new perfusion technique employed in this study using a central volume principle with deconvolution algorithm needs only 3-5 ml/s, a normal rate in routine work and much safer than the past method.[13] The injection rate used in this study was 5 ml/s, which is the minimum value needed to calculate TBF precisely with this software. If a lower injection rate, shorter injection time, or contrast material with a low iodine concentration is applied, TBF calculated with this software is not reliable because of inappropriate time-density curve. Although continuous breath holding for 40 seconds, which is the product endorsement, may be long, this duration is needed to calculate TBF under this appropriate injection rate. In addition fast imaging ability and improved image quality has also contributed to precise measurement of blood flow by decreasing noise. For these reasons, we considered perfusion CT much more practical than xenon CT. We thought that if a good correlation was found between the TBF measured by xenon CT and perfusion CT, we should use perfusion CT to calculate the TBF of pancreatic tumor. The result was, as we showed, that TBF measured by perfusion CT shows a good correlation with that obtained by xenon CT. However, one point of caution is that, when TBF is measured in tissue with permeability, such as pancreas, we need to consider leakage of contrast material into extravascular space, and complicated calculation is needed. In addition, there is no confirmed model to measure TBF, unlike that for brain, so further study is needed to quantify the TBF of tissue with permeability.

There are only a few articles about pancreatic TBF measured by perfusion CT.[30,31] Miles *et al.* reported that normal pancreatic blood flow ranged from 1.25 to 1.66 ml/min/ml. Although they also described that TBF was increased in islet cell tumor and Wilson's disease, in contrast it was decreased in a diabetic patient and in a failing pancreatic transplant.[30] Each condition included only one case, so it is difficult to evaluate the relations between these values and those diseases. Tsushima *et al.* reported that normal pancreatic TBF ranged from 0.554 to 1.698 ml/min/ml and decreased with age.[31] These reports focused on normal pancreatic TBF. The TBF measured by perfusion CT ranged from 22.1 to 50.0 ml/min/100 g in eight adenocarcinomas, which is well known as a hypovascular tumor. The scale of our value is different from that of past reports, so it is difficult to make a simple comparison among these TBF values. Our report is the first to focus on quantitative TBF of pancreatic tumor, though we had only nine cases.

One limitation of this study was the restricted slice number. Twenty millimeters (10 mm slice thickness×2 slices in perfusion CT) is not always enough to evaluate whole tumor volume. Wider detectors are becoming available in new MDCT equipment, such as the 64-channel MDCT. This means that we will be able to evaluate the TBF of whole tumors.

Radiation exposure may be another limitation. In our routine work, we usually apply a test injection method to determine the precise timing for dynamic study in a pancreatic tumor case, which needs 30 seconds of exposure, and the estimated CTDI (computed tomography dose index) volume of a timing scan in routine work is 38.2 mGy, whereas perfusion CT needs 40 seconds of continuous scanning with a low x-ray tube current. This chronological enhancement data can be employed in place of test injection data. The estimated CTDI volume of perfusion CT is 205 mGy, and that of xenon CT is 279 mGy. The CTDI volume of perfusion CT is as about five times that of the test injection scan. It is arguable whether this CTDI volume is too much or within allowance. We consider this CTDI volume within allowance, because perfusion CT is undergone in the first CT to understand the patient's condition and predict the therapeutic effect, and these are very important to evaluate the patient's prognosis.

This study was a preliminary study. Our purpose was

not the differentiation of pancreatic tumor with TBF but merely an evaluation of the correlation between the TBF of perfusion CT and that of xenon CT. The number of cases included in this study was small, and their TBF values, which reflected variable tumor vascularity, were distributed widely, leading to the wide standard deviation in the result. Although only one hypervascular tumor was included in the nine cases, the TBF correlation between perfusion CT and xenon CT is a challenge for the future.

In conclusion, the tissue blood flow of pancreatic tumors measured by xenon CT and perfusion CT techniques showed a good linear correlation. We can expect that perfusion CT based on a deconvolution algorithm may be as useful to predict the effect of pancreatic tumor treatment with anticancer drugs as xenon CT.

References

1) Postier RG. The challenge of pancreatic cancer. *Am J Surg*, 186: 579–582, 2003.
2) Egawa S, Takeda K, Fukuyama S, Motoi F, Sunamura M, Matsuno S. Clinicopathological aspects of small pancreatic cancer. *Pancreas*, 28: 235–240, 2004.
3) Abbruzzese JL. New applications of gemcitabine and future directions in the management of pancreatic cancer. *Cancer*, 95 (4 Suppl): 941–945, 2002.
4) Heinemann V. Gemcitabine: progress in the treatment of pancreatic cancer. *Oncology*, 60: 8–18, 2001.
5) El-Rayes BF, Zalupski MM, Shields AF, *et al.* Phase II study of gemcitabine, cisplatin, and infusional fluorouracil in advanced pancreatic cancer. *J Clin Oncol*, 21: 2920–2925, 2003.
6) Shukla-Dave A, Poptani H, Loevner LA, *et al.* Prediction of treatment response of head and neck cancers with P-31 MR spectroscopy from pretreatment relative phosphomonoester levels. *Acad Radiol*, 9: 688–694, 2002.
7) Sahani DV, Kalva SP, Hamberg LM, *et al.* Assessing tumor perfusion and treatment response in rectal cancer with multisection CT: initial observations. *Radiology*, 234: 785–792, 2005.
8) Gayed I, Vu T, Iyer R, *et al.* The role of 18F-FDG PET in staging and early prediction of response to therapy of recurrent gastrointestinal stromal tumors. *J Nucl Med*, 45: 17–21, 2004.
9) Kubota M, Dono K, Hashimoto K, *et al.* Evaluation between tissue blood flow of pancreatic cancer and therapeutic effect of chomoradiation therapy with Xenon CT. 58th annual meeting, The Japanese Society of Gastroenterological Surgery 2003. (in Jpse.)
10) Eastwood JD, Provenzale JM, Hurwitz LM, Lee TY. Practical injection-rate CT perfusion imaging: deconvolution-derived hemodynamics in a case of stroke. *Neuroradiology*, 43: 223–226, 2001.
11) Eastwood JD, Lev MH, Azhari T, *et al.* CT perfusion scanning with deconvolution analysis: pilot study in patients with acute middle cerebral artery stroke. *Radiology*, 222: 227–236, 2002.
12) Kudo K, Terae S, Katoh C, *et al.* Quantitative cerebral blood flow measurement with dynamic perfusion CT using the vascular-pixel elimination method: comparison with H2(15)O positron emission tomography. *AJNR Am J Neuroradiol*, 24: 419–426, 2003.
13) Lee TY. Functional CT: physiological models. *Trends in Biotechnology*, 20: S3–10, 2002.
14) World Medical Association Declaration of Helsinki: ethical principles for medical research involving human subjects. *JAMA*, 284: 3043–3045, 2000.
15) Kalender WA, Polacin A, Eidloth H, Kashiwagi S, Yamashita T, Nakano S. Brain perfusion studies by xenon-enhanced CT using washin/washout study protocols. *J Comput Assist Tomogr*, 15: 816–822, 1991.
16) Kety SS. The theory and applications of the exchange of inert gas at the lungs and tissue. *Pharmacol Rev*, 3: 1–41, 1951.
17) Fick A. Uber die Messung des Blutquantums in den Herzventrikeln Verhandl. *d phys-med Ges zu Wurzburg*, 2: 16–28, 1870. (in German)
18) Sase S. Correction method for end-tidal xenon concentration in CBF measurements with xenon-enhanced CT. *J Comput Assist Tomogr*, 20: 688–692, 1996.
19) Meyer JS, Hayman LA, Yamamoto M, Sakai F, Nakajima S. Local cerebral blood flow measured by CT after stable xenon inhalation. *AJR Am J Roentgenol*, 135: 239–251, 1980.
20) Sase S, Monden M, Oka H, Dono K, Fukuta T, Shibata I. Hepatic blood flow measurements with arterial and portal blood flow mapping in the human liver by means of xenon CT. *J Comput Assist Tomogr*, 26: 243–249, 2002.
21) Sase S, Suzuki M, Ikeda H, *et al.* Quantitative multilevel mapping of hepatic blood flow by xenon computed tomography using aorta. *J Comput Assist Tomogr*, 27: 647–651, 2003.
22) Meier P, Zierler KL. On the theory of the indicator-dilution method for measurement of blood flow and volume. *J Appl Physiol*, 6: 731–744, 1954.
23) Cenic A, Nabavi DG, Craen RA, Gelb AW, Lee TY. Dynamic CT measurement of cerebral blood flow: a validation study. *AJNR Am J Neuroradiol*, 20: 63–73, 1999.
24) Axel L. Tissue mean transit time from dynamic computed tomography by a simple deconvolution technique. *Invest Radiol*, 18: 94–99, 1983.
25) Johnson JA, Theodore AW. A model for capillary exchange. *Am J Physiol*, 210: 1299–1303, 1966.
26) Frackowiak RS, Lenzi GL, Jones T, Heather JD. Quantitative measurement of regional cerebral blood flow and oxygen metabolism in man using ^{15}O and positron emission tomography: theory, procedure, and normal values. *J Comput Assist Tomogr*, 4: 727–736, 1980.

27) Faria SC, Nq C, Phonqkitkarun S, Hess K, Mullani N, Charnsanqavi C. Comparison of blood flow measurements obtained by 15-1O-PET and functional CT in patients with solid tumors. 89th Scientific assembly and annual meeting, Radiological Society of North America 2003.
28) Winkler SS, Holden JE, Sackett JF, Flemming DC, Alexander SC. Xenon and krypton as radiographic inhalation contrast media with computerized tomography: preliminary note. *Invest Radiol*, 12: 19–20, 1977.
29) Miles KA. Measurement of tissue perfusion by dynamic computed tomography. *Br J Radiol*, 64: 409–412, 1991.
30) Miles KA, Hayball MP, Dixon AK. Measurement of human pancreatic perfusion using dynamic computed tomography with perfusion imaging. *Br J Radiol*, 68: 471–475, 1995.
31) Tsushima Y, Kusano S. Age-dependent decline in parenchymal perfusion in the normal human pancreas: measurement by computed tomography. *Pancreas*, 17: 148–152, 1998.

Puncture of Solid Pancreatic Tumors Guided by Endoscopic Ultrasonography: A Pilot Study Series Comparing Trucut and 19-Gauge and 22-Gauge Aspiration Needles

T. Itoi[1]
F. Itokawa[1]
A. Sofuni[1]
K. Nakamura[1]
A. Tsuchida[2]
K. Yamao[3]
T. Kawai[4]
F. Moriyasu[1]

Background and Study Aims: The aim of this prospective study was to compare endoscopic ultrasonography-guided Trucut needle biopsy (EUS-TNB) with EUS-guided fine-needle aspiration biopsy (EUS-FNAB) using 19- and 22-gauge needles for biopsy from different sites in patients with solid pancreatic cancers.

Patients and Methods: Sixteen consecutive patients with masses in the uncinate process (n = 3), the head (n = 5), or the body and tail (n = 8) of the pancreas underwent both EUS-TNB and EUS-FNAB. The specimens obtained were evaluated by histopathological analysis alone

Results: Tissue specimens were obtained by Trucut needle, and by 19-gauge and 22-gauge aspiration needles in 69%, 69%, and 100% of patients respectively. Sensitivity for malignancy was 69% for all needles. Tissue sampling by Trucut and by 19-gauge aspiration needle from masses in the uncinate process was impossible. The sensitivity of the Trucut and 19-gauge aspiration needles was 100% in the 11 patients with successful procedures. If Trucut or19-gauge aspiration needles had been used for body and tail masses, and the 22-gauge aspiration needle for masses in the uncinate process and head, the sensitivity for malignancy would have been 81%.

Conclusions: EUS-TNB allows reliable tissue sampling for the diagnosis of pancreatic masses, but its use is limited to lesions in the body and tail of the pancreas. EUS-FNAB using a 22-gauge needle may be useful for accurate diagnosis in some patients with masses in the uncinate process or the head of the pancreas.

Introduction

Endoscopic ultrasonography (EUS) is an essential tool in the examination of pancreatic masses [1–2]. A limitation of this technique, however, has been its inability to provide histological confirmation of diagnosis. Fine-needle aspiration biopsy (FNAB) guided by EUS (EUS-FNAB) is a safe and precise procedure for the diagnosis of pancreatic masses [3–9]. In most of these studies which reported high levels of diagnostic accuracy, a cytopathologist was present during the procedure to ensure that adequate cytological specimens were obtained. However, not all centers have a cytopathologist available during the procedure and, even if there is a cytopathologist in the endoscopy suite, the diagnosis of well-differentiated adenocarcinoma of the pancreas based on interpretation of cytological specimens alone is often difficult [10]. Investigators have therefore described and assessed the usefulness of aspiration needles of various diameters for obtaining tissue core biopsy specimens from pancreatic masses [11,12].

The recently developed EUS-applicable 19-gauge Trucut biopsy needle has been shown to obtain tissue core specimens with a high diagnostic accuracy [13,14]. In EUS-FNAB and in Trucut needle biopsy (TNB) guided by EUS (EUS-TNB), the puncture route for biopsy of pancreatic masses ranges widely, from the transgastric route to puncture through the third part of the duodenum, depending on the site of the mass. Little is currently known about how the accuracy of puncture by Trucut needle differs

Institution
[1] Fourth Department of Internal Medicine, Tokyo Medical University, Tokyo, Japan
[2] Third Department of Surgery, Tokyo Medical University, Tokyo, Japan
[3] Department of Gastroenterology, Aichi Cancer Center Hospital, Nagoya, Japan
[4] Endoscopic Center, Tokyo Medical University, Tokyo, Japan

Corresponding Author
T. Itoi, M.D. · Fourth Department of Internal Medicine, Tokyo Medical University · 6-7-1 Nishishinjuku · Shinjuku-ku · Tokyo 160-0023 · Japan · Fax: +81-3-5381-6654 · E-mail: itoi@tokyo-med.ac.jp

Submitted 17 May 2004 · Accepted after Revision 21 September 2004

Bibliography
Endoscopy 2005; 37 (4): 362–366 © Georg Thieme Verlag KG Stuttgart · New York · ISSN 0013-726X
DOI 10.1055/s-2004-826156

from site to site in pancreatic tumors. The objective of this prospective study was to compare three different needles in EUS-guided punctures of different pancreatic sites in patients with solid pancreatic cancers.

Patients and Methods

EUS-FNAB and EUS-TNB Techniques

In this study, three different needles were compared in the same patient at one procedure. We performed EUS-FNAB by using disposable 19- and 22-gauge aspiration needles (Echotip; Wilson Cook Medical Inc., Winston-Salem, North Carolina, USA) and EUS-TNB using 19-gauge Wilson Cook QuickCore Trucut needles.

The EUS-FNAB technique is well established [3–9]. Briefly, the needle was advanced into the lesion under direct EUS visualization. The central stylet was removed, a 10-ml syringe with extension tubing was attached to the hub of the needle, and suction was applied as the needle was moved backward and forward within the lesion. This extension and retraction of the needle was repeated ten times within the lesion in one puncture session. The needle was then retracted into the catheter and the entire catheter was removed. The tissue specimens obtained were fixed immediately in formalin by releasing the syringe.

The specifications and puncturing technique of the newly developed Trucut needle have been described in detail in previous reports [13,14]. In EUS-TNB, the needle was not set in the firing position before introduction into the EUS scope. After it was advanced into the target tissue under EUS visualization, its position was maintained while the spring handle was pulled back until it clicked into the firing position. The 20-mm tissue tray was then extended fully, and the spring-loaded mechanism was triggered, driving the cutting needle over the tissue tray. After firing, the biopsy needle was retracted into the sheath, and the entire assembly was removed from the EUS scope.

Because there was no cytopathologist in the endoscopy room to evaluate the quality of the aspirated specimens on-site, the adequacy of biopsy specimens obtained by EUS-FNAB and EUS-TNB was evaluated by gross inspection alone. The procedure finished after such inspection confirmed the presence of tissue. If a needle was not able to exit from the channel at the scope tip due to the degree of the angle, the needle was retracted and the device was set at a new angle.

Comparison Between EUS-TNB and EUS-FNAB

This study was performed between July 2003 and October 2003 in 16 consecutive hospitalized patients with pancreatic cancer (ten men, six women; mean age 62, range 58–80), who underwent both EUS-FNAB and EUS-TNB. All the pancreatic masses had been discovered before this study began by extra-abdominal ultrasound, computed tomography, clinical symptoms of weight loss, abdominal pain, and obstructive jaundice, and the finding of a high serum level of carbohydrate antigen 19–9. The site of pancreatic cancer was the uncinate process in three patients, the head of the pancreas in five patients and the body and tail region in eight patients.

All patients received oropharyngeal anesthesia and were sedated with injections of 3–10 mg diazepam. Evaluation of the pancreatic mass for staging was performed first, using a radial scanning endo echoscope (GF-UM-C2000; Olympus Optical, Co., Tokyo, Japan). EUS-FNAB was then performed using the Olympus GF-UCT2000 curved linear array echo endoscope. A transgastric approach was used for lesions in the body and tail region of the pancreas, and the transduodenal approach was used for lesions in the head and uncinate process of the pancreas. All patients agreed to undergo this procedure using the three different needles and gave written informed consent to their participation in the study. The study was approved by the Institutional Review Board of our institution.

Histological Diagnosis

The samples obtained in this study were evaluated by histopathological analysis alone. Histopathological examination of biopsy specimens was performed using standard hematoxylin and eosin (H & E) staining. The maximum length of each sample was measured, excluding blood clots. The histological findings were classified as malignant, atypical, or benign. When representative material was not present, the specimens were interpreted as inadequate. Two expert pathologists, who did not have any clinical information about the patients, reviewed the histological specimens separately.

Data Analysis

The sensitivity of EUS-FNAB or EUS-TNB and the resulting H & E-stained specimens was determined by comparing their results with final surgical or autopsy pathological diagnoses, or with the results of clinical follow-up of at least 10 months' duration. In the latter case, lesions were considered to be malignant if there was clinical progression of disease or if there was a response to chemotherapy. The size of the biopsy specimens was carefully calculated by microscopic measurement. Indeterminate histological results (an inadequate specimen or atypical appearances) were considered to be errors when sensitivity was determined. Intragroup comparisons were made using the chi-squared test.

Results

EUS-FNAB and EUS-TNB were performed, with no procedure-related complications, in 16 patients in whom a pancreatic cancer had been visualized by conventional EUS. The initial results of these procedures are summarized in Table **1**. The mean size of all the masses in the whole group of patients was 36.3 mm, and the mean sizes of the masses in the uncinate process, the head, and the body and tail regions of the pancreas were 27.7 mm, 36.6 mm, and 39.3 mm, respectively.

Pancreatic tissue specimens were obtained by Trucut needle biopsy in 11 of the 16 patients (69%) (Table **1**, Figure **1**). Tissue sampling from masses in the uncinate process of the pancreas using a Trucut needle was impossible in all three patients. Although these masses were visualized on the puncture route, before the needle was passed into the accessory channel, in two of these three patients, images of the mass disappeared from the puncture route because deflection of the tip of the endoscope

Table 1 Initial results of endoscopic ultrasonography-guided Trucut needle biopsy (EUS-TNB) and endoscopic ultrasonography-guided fine-needle aspiration biopsy (EUS-FNAB) of solid pancreatic masses in 16 patients

Location of tumor	*No. of cases*	*Route of needle passage*	*Mean size of mass (range), mm*	*Success rate (mean no. of passes)*		
				EUS-TNB with 19-gauge Trucut	*EUS-FNAB with 19-gauge Echotip*	*EUS-FNAB with 22-gauge Echotip*
Uncinate process	3	Transduodenal	27.7 (25–30)	0/3 (0)	0/3 (0)	3/3 (1.7)
Head	5	Transduodenal	36.6 (34–40)	3/5 (1.4)	3/5 (1.6)	5/5 (1.6)
Body/tail	8	Transgastric	39.3 (24–52)	8/8 (1)	8/8 (1.1)	8/8 (1.4)
Total	16		36.3	11/16 (1.2)	11/16 (1.3)	16/16 (1.5)
Mean size of specimens (range), mm				3.4 (2.0–5.2)	1.6 (0.8–2.4)	0.7 (0.3–1.2)

Table 2 Histological diagnosis of the biopsies obtained by EUS-TNB and by EUS-FNAB

Histological diagnosis	*EUS-TNB 19-gauge Trucut needle*	*EUS-FNAB 19-gauge Echotip needle*	*22-gauge Echotip needle*
Benign	0	0	0
Malignant	11 (100%)*	11 (100%)†	11 (69%)*†
Atypical	0	0	2 (12%)
Inadequate specimen	0	0	3 (19%)
Total	11	11	16

* $P < 0.05$, chi-squared test (Trucut vs. 22-gauge Echotip).
† $P < 0.05$, chi-squared test (19-gauge Echotip vs. 22-gauge Echotip).

was restricted by the advance of the needle; in the other patient, the mass was visualized on the puncture route but tissue sampling was impossible due to the strong resistance encountered when the needle was advanced. Tissue specimens were obtained in three of the five patients (60%) with masses in the pancreatic head; in the remaining two patients, tissue specimens could not be obtained because the advancing needle met with strong resistance. Tissue specimens were obtained from all patients with masses of the pancreatic body and tail region. Similar results were obtained using the 19-gauge aspiration needle. In contrast, tissue specimens or fragments were obtained by the 22-gauge needle from all patients, regardless of the location of their pancreatic mass (Table **1**).

The mean size of tissue specimens obtained by Trucut needle was 3.4 mm. The 19-gauge aspiration needle was equally successful in obtaining tissue samples (in 11/16 patients), but these specimens were smaller (mean size 1.6 mm) than those obtained by the Trucut needle. Tissue fragments were aspirated in all 16 patients by the the 22-gauge aspiration needle (Figure **2**). The mean size of these fragments was 0.7 mm. The mean size of the tissue samples obtained with the Trucut needle was therefore greater than the mean size of samples obtained using the aspiration needles.

The mean number of passes of the three different needles in patients in whom the needle could be advanced was 1.2 for the Trucut needle, 1.3 for the 19-gauge Echotip needle, and 1.5 for the 22-gauge Echotip needle. The mean number of needle passes in cases in which the needle could be advanced in patients with masses in the uncinate process was 1.7. In patients with masses in the head of the pancreas, the mean number of needle passes for the three needles showed similar results (Trucut, 1.4; 19-gauge Echotip, 1.6; and 22-gauge Echotip, 1.6). In patients with masses in the body and tail region, the mean number of passes was 1.0 for the Trucut needle, 1.1 for the 19-gauge Echotip needle, and 1.4 for the 22-gauge Echotip needle, respectively. There was a statistically significant difference between the Trucut and 22-gauge aspiration needles in terms of the number of passes ($P < 0.05$).

Table **2** shows the histological diagnosis by EUS-FNAB and EUS-TNB. The sensitivity for malignancy was 69% (11/16) regardless of the needles used. When the calculation of the sensitivity was limited to the 11 patients in whom the procedure was technically possible, both TNB and FNAB using a 19-gauge needle provided a correct diagnosis in all cases (11/11). There was a statistical difference between these results and the results of FNAB using a 22-gauge needle, which provided a correct diagnosis in 11 patients of the 16 in whom the procedure was technically feasible (69%, $P < 0.05$) (see Table **2**). FNAB using a 22-gauge needle produced three inadequate and two atypical samples. The 22-gauge aspiration needle provided a correct diagnosis in two out of three patients with masses in the uncinate process (67%), in three of five patients with masses in the pancreatic head (60%), and in six out of eight patients with masses in the body and tail region (75%). Among the five patients with indeterminate specimens, the final histological diagnosis, made from EUS-TNB specimens, was well-differentiated pancreatic adenocarcinoma in four patients and moderately differentiated adenocarcinoma in one patient.

Discussion

Theoretically, a pancreatic core biopsy specimen has many advantages compared with a cytological specimen in terms of improving the diagnostic yield. In the present study, because a cytopathologist was not present during the procedures, we assessed the diagnostic accuracy using the three different needles by histological analysis alone. To date there have been no reports on

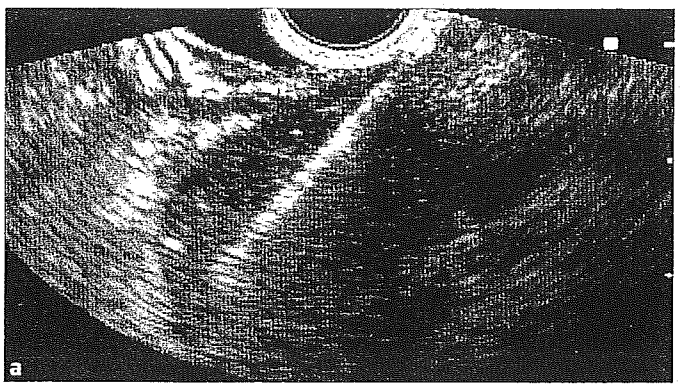

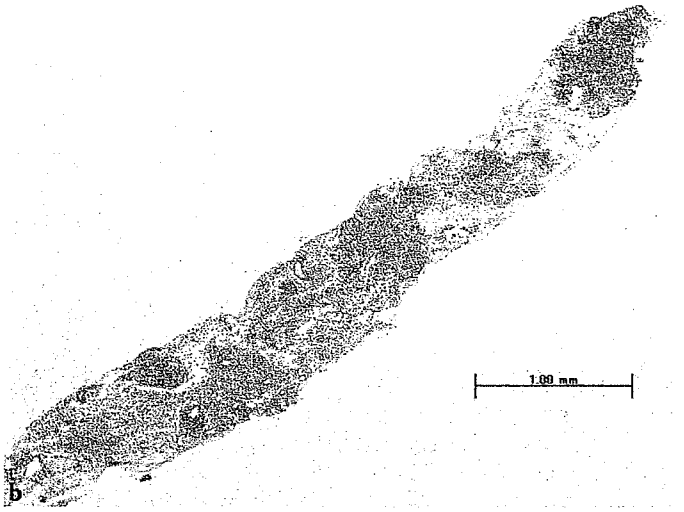

Figure 1 Trucut biopsy of a pancreatic mass. **a** The Trucut needle is identified by its strong echo, advancing into the mass under visualization by direct linear array endoscopic ultrasound. **b** Histological view of tissue obtained by Trucut needle biopsy guided by endoscopic ultrasonography after staining with hematoxylin and eosin [H & E], showing poorly differentiated adenocaricnoma of the pancreas (× 4, bar length 1 mm).

Figure 2 Photomicrograph of representative tissue samples obtained by endoscopic ultrasonography-guided fine-needle aspiration biopsy using a 22-gauge needle (H & E, × 4, bar length 1 mm).

how the accuracy of puncture with Trucut and with small- and large-caliber aspiration needles differs according to the site of the tumor in patients with pancreatic masses, although some investigators have tried to assess how to use different needles in small numbers of cases [13,14].

In this study we used three different needles: 69% of the tissue specimens obtained by Trucut and by 19-gauge aspiration needles were found to be analyzable; the rate for the 22-gauge needle was 100%. This result for the 22-gauge needle was slightly higher than the 88% to 90% rates previously reported [3–9], but the results for the 19-gauge aspiration needle and the Trucut needle were lower than those found previously. The cause of the lower numbers of analyzable specimens obtained by these two needles may be related to the location of the pancreatic masses. For masses in the uncinate process, we were unable to perform either EUS-FNAB with the 19-gauge needle or EUS-TNB. Although the small number of patients and the smaller size of uncinate process masses may have a bearing on these poor results, we thought that the main factor was that the degree of deflection of the endoscope tip required to bring the pancreatic masses into an appropriate position precluded extension of the needle from the accessory channel. It was also difficult to obtain tissue specimens from the head of the pancreas. Similar problems and results have been described when large-caliber needles were used for EUS-FNAB or EUS-TNB [11–14]. Binmoeller et al. [11] used an 18-gauge aspiration needle to biopsy pancreatic masses and obtained analyzable histological specimens from 78% of patients (31/40), compared with adequate cytology specimens from 85% (34/40). They also described failures with FNAB in five patients. Although we do not know about the location of masses in these patients, they reported that all four patients with false-negative FNAB results had masses in the head of the pancreas. As for 19-gauge Trucut needles, Larghi et al. [14] reported that analyzable tissue specimens were obtained from 17 out of 23 pancreatic masses (74%), of which four were masses of the head of the pancreas (4/10, 40%) and 13 were masses of the body and tail region (13/13, 100%). These data were similar to our results. Although the results of our study showed no difference between the 19-gauge aspiration needle and the Trucut needle, our study and other studies [12–14] suggest that indications for using large-caliber needles like the 19-gauge needles, especially the current Trucut needle, for lesions in the uncinate process and the head of the pancreas that are approached transduodenally are limited, and that these needles are better suited for biopsy of lesions in the body and tail of the pancreas that are approached transgastrically.

In the present study, the sensitivity for malignancy was 69% for all three needles. In previous reports, the sensitivity for detection of solid pancreatic neoplasms by histological specimens obtained using 18- and 22-gauge aspiration needles was 53% (9/17) [11] and 74% (55/74) [12], respectively. Both these and our own sensitivity results are lower than those achieved in previous large series in which results were based on cytological diagnosis with a cytopathologist present during the procedure [3–9]. In the case of the 22-gauge needle, this discrepancy may be due mainly to the existence of a cytopathologist. It is noteworthy that the sensitivity was 100% for both EUS-TNB and EUS-FNAB using 19-gauge needles when the calculation of the sensitivity was limited to the 11 patients in whom the procedure was technically possible. This result is similar to results reported previously for 19-gauge Trucut needles [13,14]. In these studies, the sensitivity of Trucut needle biopsy in patients with pancreatic neoplasms was 67% (2/3) [13] and 67% (8/12) [14]. The sensitivity of EUS-TNB has also been found to be higher than that of EUS-FNAB [14,15]. Interestingly, if we had used 19-gauge aspiration or Trucut needles in patients with masses of the body and tail regions of the pancreas and 22-gauge aspiration needles in

patients with the masses of the uncinate process and pancreatic head, the sensitivity would have been 81% (13/16).

The mean number of passes of the Trucut needle was no different from the mean number of passes of the aspiration needles in biopsies of the pancreatic head masses. However, the number of passes of the Trucut needle was lower than that of the 22-gauge needle for masses in the body and tail region of the pancreas. In addition, during the EUS-TNB procedure, there was no need to move the needle in the mass, resulting in shorter procedure times compared with biopsies with the aspiration needles, in which the extension–retraction maneuver had to be repeated ten times per pass. As previously reported, this result points to the usefulness of the Trucut needle, which provides adequate biopsy samples with one puncture alone, compared with the aspiration needle, especially in the biopsy of pancreatic masses that bleed easily [13,14]. In the present study, FNAB by 22-gauge needle produced three inadequate and two atypical samples. In four of these five patients, a diagnosis of well-differentiated pancreatic adenocarcinoma was made using specimens obtained by Trucut needle.

In the present study, the mean size of the specimens obtained by the 22-gauge needles was 0.7 mm, which was less than the mean size of the specimens obtainable with 19-gauge aspiration and Trucut needles. The larger specimens obtained by Trucut needle may be helpful for the diagnosis of malignancy. In the future, furthermore, we believe that large tissue samples obtained by EUS-TNB may contribute to the therapy of pancreatic diseases because of their usefulness for gene or immunohistochemical analysis.

In the current study, no early or late procedure-related complications occurred with any of the needles. In general, EUS-FNAB has proved to be remarkably safe in experienced hands, with reported complication rates of 2.5% or less [3,4,6,9]. EUS-TNB caused no complications in previous reports [13,14]. The lack of complications in this study may be related to the lower number of passes.

In conclusion, EUS-TNB provides for reliable tissue sampling for the diagnosis of pancreatic masses with fewer punctures than are needed for conventional EUS-FNAB, though it would be necessary to accumulate greater numbers of clinical cases to assess this procedure more thoroughly. Its indications, however, are limited, because it cannot be used for lesions in the uncinate process of the pancreas. Trucut needle biopsy is best for lesions in the body and tail regions of the pancreas. Its indications for lesions in the head of the pancreas may also be restricted, depending on tumor location and size. In such cases, EUS-FNAB using a 22-gauge needle may be useful for accurate diagnosis.

References

[1] Rösch T, Braig C, Gain T et al. Staging of pancreatic and ampullary carcinoma by endoscopic ultrasonography: comparison with conventional sonography, computed tomography, and angiography. Gastroenterology 1992; 102: 188–199

[2] Yasuda K, Mukai H, Fujimoto S et al. The diagnosis of pancreatic cancer by endoscopic ultrasonography. Gastrointest Endosc 1988; 34: 1–8

[3] Wiersema MJ, Vilmann P, Giovannini M et al. Endosonography-guided fine-needle aspiration biopsy: diagnostic accuracy and complication assessment. Gastroenterology 1997; 112: 1087–1095

[4] Yamao K, Ohashi K, Mizutani S et al. Endoscopic ultrasound-guided fine-needle aspiration (EUS-FNA) for the diagnosis of digestive diseases. Endoscopy 1998; 30: A176–A178

[5] Lai R, Stanley MW, Bardales R et al. Endoscopic ultrasound-guided pancreatic duct aspiration: diagnostic yield and safety. Endoscopy 2002; 34: 715–720

[6] Chang KJ, Nguyen PM, Erickson RA et al. The clinical utility of endoscopic ultrasound-guided fine-needle aspiration in the diagnosis and staging of pancreatic carcinoma. Gastrointest Endosc 1997; 45: 387–393

[7] Bhutani MS, Hawes RH, Baron PL et al. Endoscopic-ultrasound fine-needle aspiration of malignant pancreatic lesions. Endoscopy 1997; 29: 854–858

[8] Das A, Chak A. Endoscopic ultrasonography. Endoscopy 2004; 36: 17–22

[9] Giovannini M, Seitz JF, Monges G et al. Fine-needle aspiration cytology guided by endoscopic ultrasonography: results in 141 patients. Endoscopy 1995; 27: 171–177

[10] Yeaton P, Sears RJ, Ledent T et al. Discrimination between chronic pancreatitis and pancreatic adenocarcinoma using artificial intelligence-related algorithms based on image cytometry-generated variables. Cytometry 1998; 32: 309–316

[11] Binmoeller KF, Thul R, Rathod V et al. Endoscopic ultrasound-guided, 18-gauge, fine-needle aspiration biopsy of the pancreas using a 2.8-mm channel convex echo endoscope. Gastrointest Endosc 1998; 47: 121–127

[12] Voss M, Hammel P, Molas G et al. Value of endoscopic ultrasound-guided fine-needle aspiration biopsy in the diagnosis of solid pancreatic masses. Gut 2000; 46: 244–249

[13] Levy MJ, Jondal ML, Clain LPNJ et al. Preliminary experience with an EUS-guided Trucut biopsy needle compared with EUS-guided FNA. Gastrointest Endosc 2003; 57: 101–106

[14] Larghi A, Verna EC, Stavropoulos SN et al. EUS-guided Trucut needle biopsies in patients with solid pancreatic masses: a prospective study. Gastrointest Endosc 2004; 59: 185–190

J Gastroenterol 2005; 40:518–525
DOI 10.1007/s00535-005-1578-z

Journal of Gastroenterology

© Springer-Verlag 2005

Differential diagnosis of pancreatic tumors using ultrasound contrast imaging

Atsushi Sofuni, Hiroko Iijima, Fuminori Moriyasu, Daijyu Nakayama, Masafumi Shimizu, Kazuto Nakamura, Fumihide Itokawa, and Takao Itoi

Fourth Department of Internal Medicine, Tokyo Medical University, 6-7-1 Nishishinjuku, Shinjyuku-ku, Tokyo 160-0023 Japan

Background. The development of equipment and contrast agents for ultrasound imaging has contributed to major breakthroughs in the diagnosis of pancreatic tumors. We aimed to determine the diagnostic effectiveness of contrast ultrasound with Levovist, using the Agent Detection Imaging (ADI) technique, in 50 patients with pancreatic tumors. ***Methods.*** We studied 50 cases of histologically proven pancreatic disease; 39 carcinomas, 2 endocrine tumors, 4 intraductal papillary mucinous carcinomas (IPMCs), and 5 cases of tumor-forming pancreatitis (TFP). Vascular and perfusion images of contrast-enhanced ultrasound (CE-US) were used for the evaluation of tumor vascularity and parenchymal perfusion of the tumor, respectively. The hemodynamics of the tumor, and the diagnostic capacity of CE-US were compared with those shown by computed tomography (CT). The histological diagnosis in all cases was made from either biopsy or surgical specimens. ***Results.*** Thirty-four cases of pancreatic carcinoma (87%) showed a hypovascular and hypoperfusion pattern. The endocrine tumors showed a heterogeneous hypervascular and hyperperfusion pattern. All IPMC cases showed hypervascularity of the nodules inside the tumors. TFP showed an isovascular and homogeneous isoperfusion pattern. When tumors showing a hypovascular or hypoperfusion pattern on CE-US were diagnosed as carcinomas, 34 of the 39 carcinomas (87%) fit this criterion, with a 95% confidence interval (CI) of 73%–96%, whereas, on CT, 31 of the 39 were diagnosed as carcinoma; (sensitivity, 79%). The sensitivity and accuracy of CT were inferior to those of CE-US. Results of comparison between the CE-US findings and the histological diagnosis were as follows. The one papillary adenocarcinoma showed a hypervascular and hyperperfusion pattern; the 32 well or moderately differentiated adenocarcinomas showed a hypovascular and hypoperfusion pattern; and in the poorly differentiated adenocarcinomas, 2 cases of scirrhous type showed a hypovascular and hypoperfusion pattern, and the 4 cases of medullary type showed an isovascular and isoperfusion pattern. ***Conclusions.*** The differences in vascularity of pancreatic carcinomas depicted by CE-US were associated well with differences in histology. CE-US, by the ADI technique, is useful for the diagnosis of pancreatic tumors.

Key words: ultrasound contrast imaging, Agent Detection Imaging, pancreatic tumor, grade of histological differentiation

Introduction

The capacity to diagnose pancreatic tumors has made major progress with the advent and spread of various diagnostic imaging techniques, such as ultrasound (US), computed tomography (CT), CT-guided fine-needle aspiration biopsy (CT-FNAB), endoscopic US (EUS), and EUS-FNAB.[1–8] Also included among these techniques is contrast-enhanced US (CE-US), which is performed in connection with angiography, using hand-agitated carbon dioxide microbubbles. This latter technique has been reported to be useful not only in the diagnosis of hepatic tumors[9,10] and gallbladder[11] lesions but also for pancreatic lesions.[12] Conventional power Doppler US and tissue harmonic imaging (THI) do not need a contrast agent and are noninvasive and easy to carry out, and thus have played a major role in the

Received: August 4, 2004 / Accepted: January 28, 2005
Reprint requests to: A. Sofuni
This paper was given as an oral presentation at the Tenth United European Gastroenterology Week (Geneva, Switzerland, 2002), and received an award as one of the "Best 200 Abstracts". A poster presentation of the paper was made at the 11th United European Gastroenterology Week (Madrid, Spain, 2003).

Table 1. CE-US imaging with ADI in 50 pancreatic tumors

Diagnosis	No. of cases	Vascular image (n = 50)			Perfusion image (n = 46)		
		Hypo	Iso	Hyper	Hypo	Iso	Hyper
Pancreatic carcinoma	39	34 (87%)	4 (10%)	1 (3%)	34 (87%)	4 (10%)	1 (3%)
Endocrine tumor	2	0 (0%)	0 (0%)	2 (100%)	0 (0%)	0 (0%)	2 (100%)
IPMC	4	0 (0%)	0 (0%)	4 (100%)	NA	NA	NA
TFP	5	1 (20%)	4 (80%)	0 (0%)	0 (0%)	5 (100%)	0 (0%)

IPMC, intraductal papillary mucinous carcinoma; TFP, tumor-forming pancreatitis; NA, not available

diagnosis of pancreatic lesions from the viewpoint of assessment of vascularity.[13,14]

Recently, intravenous contrast agents for US, such as Levovist (Schering, Berlin, Germany) have been developed, and it has become possible to investigate not only the vascularity of the lesion but also the perfusion of the lesion noninvasively.

The effectiveness of CE-US techniques, using Levovist, has been reported in the diagnosis of hepatic lesions.[15–24] In particular, Agent Detection Imaging (ADI), which has been developed by Siemens-Acuson (Mountainview, CA, USA), has a high sensitivity for Levovist and is expected to be effective in the diagnosis of liver diseases.[21,22]

In pancreatic diseases, however, the effectiveness of CE-US has only been reported with color Doppler imaging,[25] pulse inversion harmonics (PIH),[26] and coded phase inversion harmonic imaging.[27]

In this study, the diagnostic effectiveness of a technique using Levovist and ADI was evaluated by comparing the results, reviewed by blinded experts, with those of histologically proven pancreatic tumors. This differential diagnosis of pancreatic tumors, using CE-US with ADI, compared with histological evaluation, has not been reported before.

Patients, materials, and methods

We studied the pancreatic tumors of 50 patients who had been treated in our hospital during the period from September 2000 to December 2002. There were 39 pancreatic carcinomas, 2 endocrine tumors, 4 intraductal papillary mucinous carcinomas (IPMCs), and 5 cases of tumor-forming pancreatitis. The histological diagnosis was obtained from EUS-FNAB in 30 patients, endoscopic and percutaneous biopsy in 9, and surgical specimens in 11. Also, 6 healthy volunteers were investigated as a control group.

The US equipment used was a Sequoia 512 (Siemens-Acuson; Mountainview, CA, USA), and the probe was a convex array electronic transducer 4CI. Levovist (2.5 g) was prepared at a dose of 300 mg/ml, and a bolus of 7 ml was injected through the median cubital vein, at a speed of 1 ml/s. The imaging mode used was the ADI technique. The parameters for imaging included: mechanical index (MI), 1.4–1.9; transmission frequency, 2.0 MHz; and receiving frequency, 4.0 MHz.

After the detailed observation of the lesion in B-mode, vascular images were depicted for 60 s after the injection of the contrast agent, at the speed of 5 frames/s (fps) with breath-holding, focusing on the blood-flow dynamics in the lesion and surrounding pancreatic tissue. Subsequently, perfusion images were depicted for 180 s after the injection of the contrast agent, with intermittent transmissions for periods of 2–10 s to observe the enhancement of the lesion.

In both the vascular and the perfusion images, the blood-flow signal in the tumor was compared with that in nontumor regions and classified into patterns, depending on the signal intensity, as hypervascular and hyperperfusion: isovascular and isoperfusion; or hypovascular and hypoperfusion. The results were categorized into three groups; "hyper", "iso", and "hypo" signals, respectively (Table 1).

Images were recorded for tumors in all 50 patients, and the data were interpreted by three blinded readers (D.N., H.I., and F.M.), who with expertise in contrast US studies. These readers were not informed regarding the patients' backgrounds or diagnoses.

The sensitivity, specificity, positive predictive value (PPV), negative predictive value (NPV), and accuracy for diagnosis were calculated. The cutoff criterion was that the hypovascular or hypoperfusion pattern was diagnosed as pancreatic carcinoma; the 95% confidence interval (CI) was calculated using Microsoft Excel (version 5.0; Redmond, WA, USA). The hemodynamics of the tumor and the diagnostic capacity of CE-US were compared with those of CT.

This study was approved by the Tokyo Medical University Institutional Ethics Review Board for Clinical Studies. All subjects gave their informed consent for the study.

Results

The locations of the tumors were: the head (26 cases), uncus (4 cases), body (7 cases), and tail (13 cases).

All these tumors could be imaged by conventional US. The size of the tumors ranged from 12 mm to 83 mm (average, 35.1 mm) in diameter.

In the 6 healthy volunteers, the pancreas image started to become enhanced in 10–20 s, and was homogeneously enhanced for 30 s on average.

Table 1 shows the results of the CE-US imaging. On vascular imaging, the tumors showed a hypervascular pattern in 7 cases, isovascular pattern in 8 cases, and hypovascular pattern in 35 cases. On perfusion imaging, the tumor showed a hypervascular pattern in 3 cases, isovascular pattern in 9 cases; and hypovascular pattern in 34 cases. There was no parenchyma to be visualized in the 4 cases of IPMC.

The vascular images of the 39 pancreatic carcinomas were classified into three patterns: hypovascular (Fig. 1b) in 34 cases (87%); heterogeneous isovascular (Fig. 2b) in 4 cases; and hypervascular (Fig. 3b) in 1 case.

The perfusion images were classified into three patterns: hypoperfusion (Fig. 1c) in 34 cases (87%) heterogeneous isoperfusion (Fig. 2c) in 4 cases, and hypervascular (Fig. 3c) in 1 case.

In all tumors, the vascular images and perfusion images coincided in enhancement behavior. The tumors with a hypovascular and hypoperfusion pattern did not totally lack the flow signal, but rather, exhibited weak punctate or fine arborizing patterns of flow signals inside the tumor (Fig. 1b, c).

The two pancreatic endocrine tumors showed a heterogeneous hypervascular and hyperperfusion pattern throughout the tumor (Fig. 4)

All IPMCs had heterogeneous, hypervascular nodules on the vascular images (Fig. 5).

Tumor-forming pancreatitis showed the following vascular image patterns: isovascular (Fig. 6b) (4 cases; 80%) and hypovascular (1 case; 20%). All cases of tumor-forming pancreatitis showed a diffuse and homogeneous isoperfusion pattern on perfusion imaging (Fig. 6c).

The sensitivity, specificity, and accuracy of the CE-US were calculated as follows. The criterion was that, among the 46 cases of pancreatic tumors (excluding IPMC), those cases with a hypovascular and hypoperfusion pattern on CE-US were diagnosed as pancreatic carcinoma. This criterion fitted in 34 of the 39 pancreatic carcinomas (87%; 95% confidence interval [CI], 73%–96%). For the vascular imaging, the sensitivity was 87.2% (34/39); the specificity was 85.7% (6/7); the PPV was 97.1% (34/35); the NPV was 54.5% (6/11); and the accuracy was 87.0%. For the perfusion imaging, the sensitivity was 87.2% (34/39); the specificity was 100% (7/7); the PPV was 100% (34/34); the NPV was 58.3% (7/12); and the accuracy was 89.1%.

The histological classification of the pancreatic carcinomas was: papillary adenocarcinoma in 1 case; well or moderately differentiated adenocarcinoma in 32 cases; and poorly differentiated adenocarcinoma in 6 cases.

The papillary adenocarcinoma showed a hypervascular and hyperperfusion pattern; all 32 well or moderately differentiated adenocarcinomas showed a hypovascular and hypoperfusion pattern; 2 of the 6 poorly differentiated adenocarcinomas were scirrhous type and showed a hypovascular and hypoperfusion pattern, and the 4 other poorly differentiated adenocarcinomas were medullary type and showed an isovascular and isoperfusion pattern.

A flow chart of the for the diagnosis of pancreatic tumors by CE-US is shown in Fig. 7.

Table 2 shows a comparison of vascularity on CT and CE-US in the 50 pancreatic tumors examined. All pancreatic tumors were depicted on CE-US. However, helical CT depicted 46 of the 50 tumors and failed to detect 4 tumors, which were all pancreatic carcinomas of 2 cm or less in size. The detection rate of pancreatic carcinoma was 89.7% on CT, compared with a detection rate of 100% on CE-US. When cases showing hypovascularity on CT were diagnosed as pancreatic carcinoma, the sensitivity was 79.5%; the specificity was 100%; the PPV was 100%; the NPV was 57.9%; and the accuracy was 84.0%. The rate of concordance of the enhancement pattern between CE-US and CT was 86% (43/50 tumors). Two of the 39 pancreatic carcinomas (5.1%), 1 case of TFP, and all cases of IPMC showed different enhancement patterns on CE-US and CT.

Discussion

Several diagnostic modalities have been used for the contrast imaging of pancreatic tumors. X-ray angiography or US angiography with carbon dioxide microbubbles have been used for the evaluation of vascularity (vascular imaging), and dynamic CT has been used for the evaluation of parenchymal perfusion.

Another diagnostic modality, CE-US, has been performed simultaneously with X-ray angiography, using hand-agitated carbon dioxide microbubbles, for the diagnosis and evaluation of blood flow to pancreatic tumors.[12] Large carbon dioxide microbubbles, 30–40 μm in diameter, are used in this technique. Therefore, blood vessels that are larger than arterioles can be visualized by embolizing them. This technique is therefore not suitable to visualize parenchymal perfusion, although it effectively provides a birds-eye view of the vasculature of the lesion.[15]

Levovist microbubbles, on the other hand, are microbubbles of 2–3 μm in diameter, which can easily pass through the capillaries,[16] thus allowing evaluation of the actual perfusion of the organ or lesion as well as

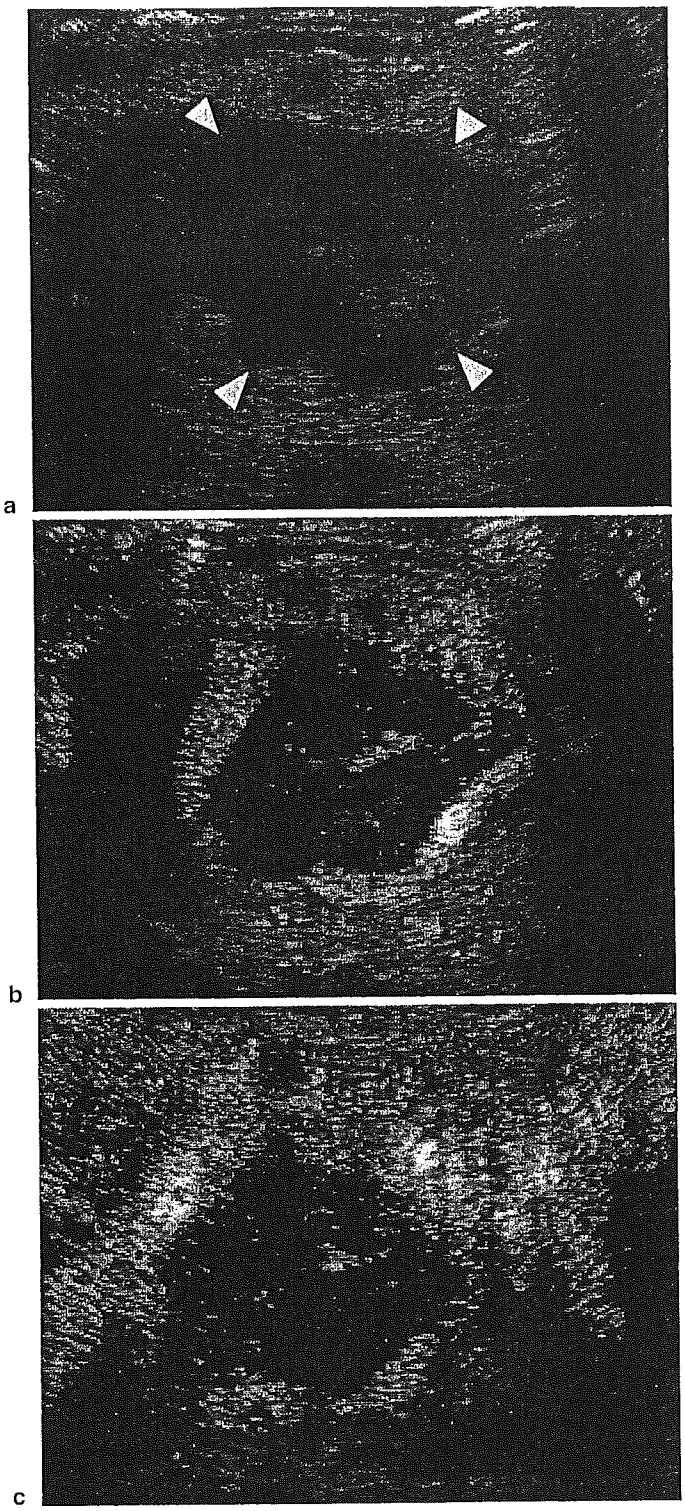

Fig. 1a–c. A case of moderately differentiated adenocarcinoma of the pancreatic head. B-mode ultrasound (US) showed a hypoechoic tumor **(a)**, and contrast-enhanced (CE)-US revealed a hypovascular pattern and punctate flow signals throughout the lesion both on the vascular image **(b)** and the perfusion image **(c)**. *Arrowheads* in **a** show the outline of the tumor

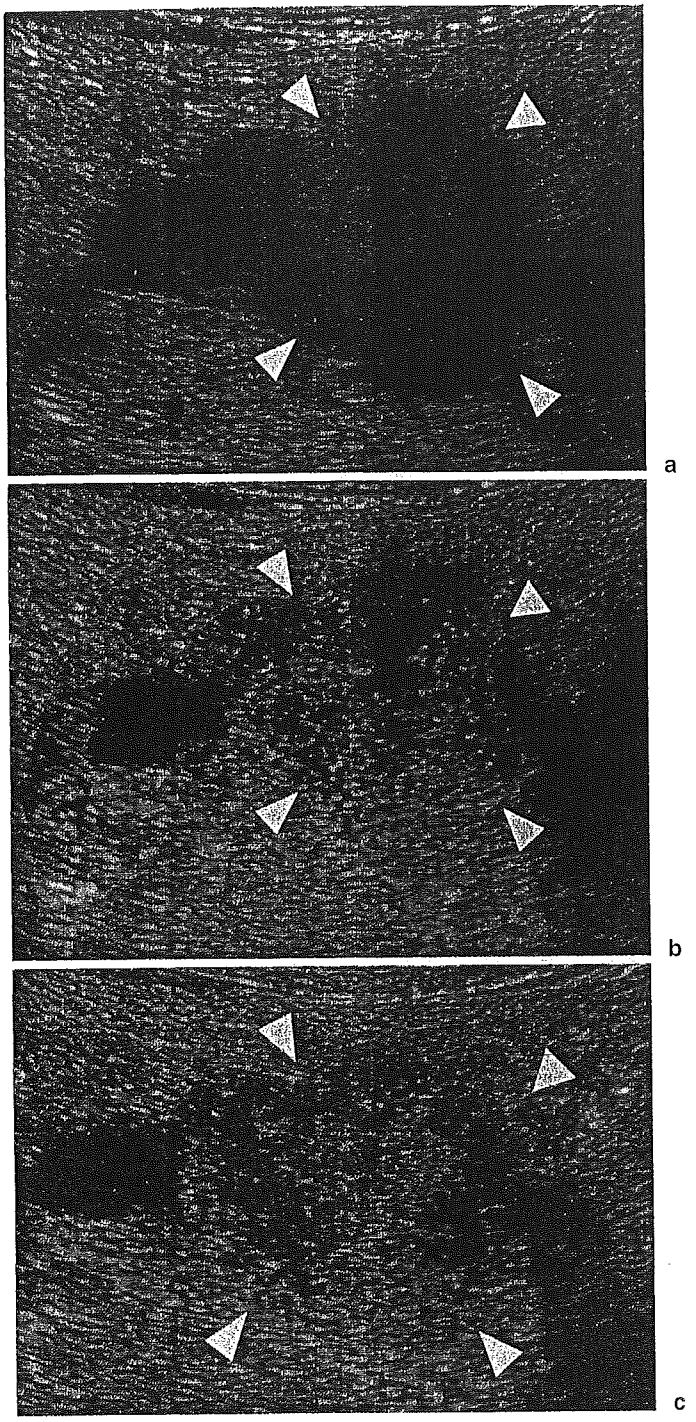

Fig. 2a–c. A case of poorly differentiated adenocarcinoma seen in the tail of the pancreas. B-mode US showed a hypoechoic tumor **(a)**, and CE-US revealed a heterogeneous isovascular pattern throughout the lesion both on the vascular image **(b)** and the perfusion image **(c)**. *Arrowheads* in **a–c** show the outline of the tumor

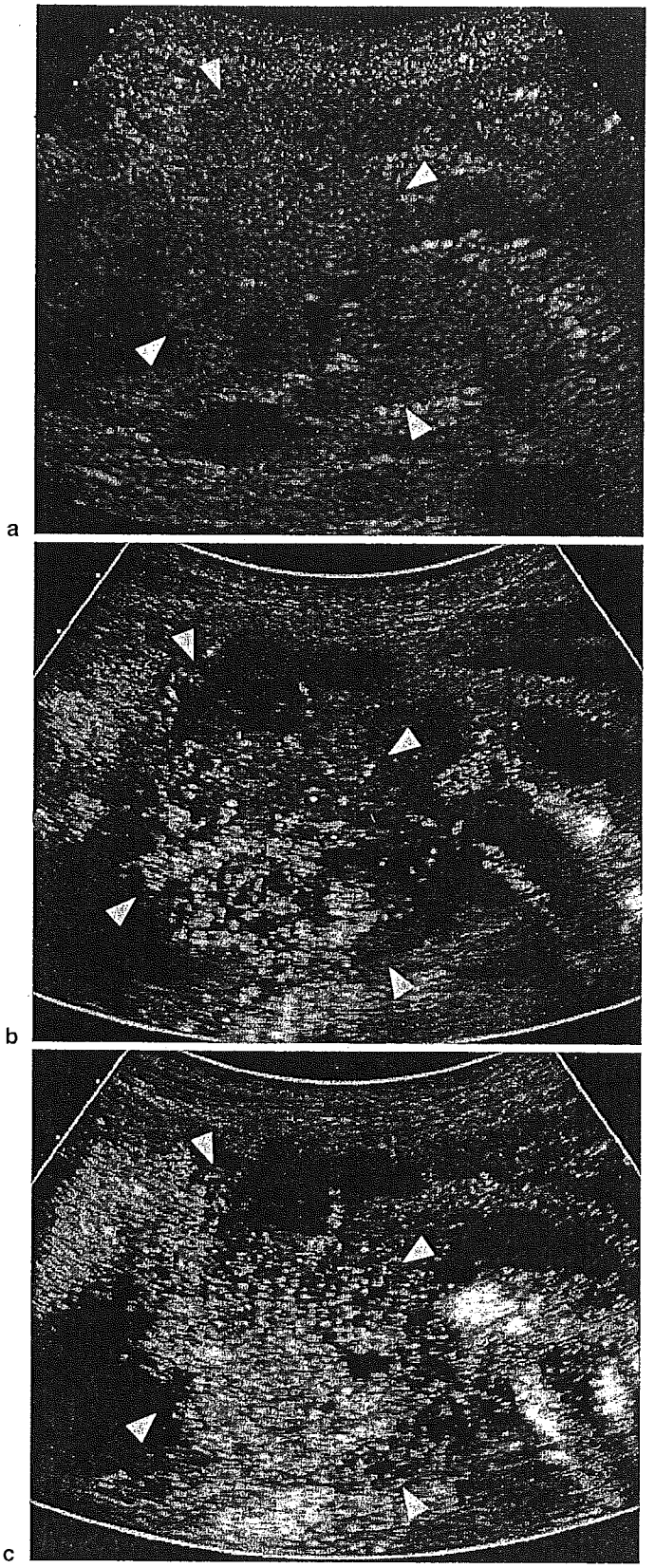

Fig. 3a–c. A case of papillary adenocarcinoma of the pancreatic head. B-mode US showed a hypoechoic tumor **(a)**, and CE-US revealed a heterogeneous hypervascular pattern throughout the lesion, both on the vascular image **(b)** and the perfusion image **(c)**. *Arrowheads* in **a–c** show the outline of the tumor

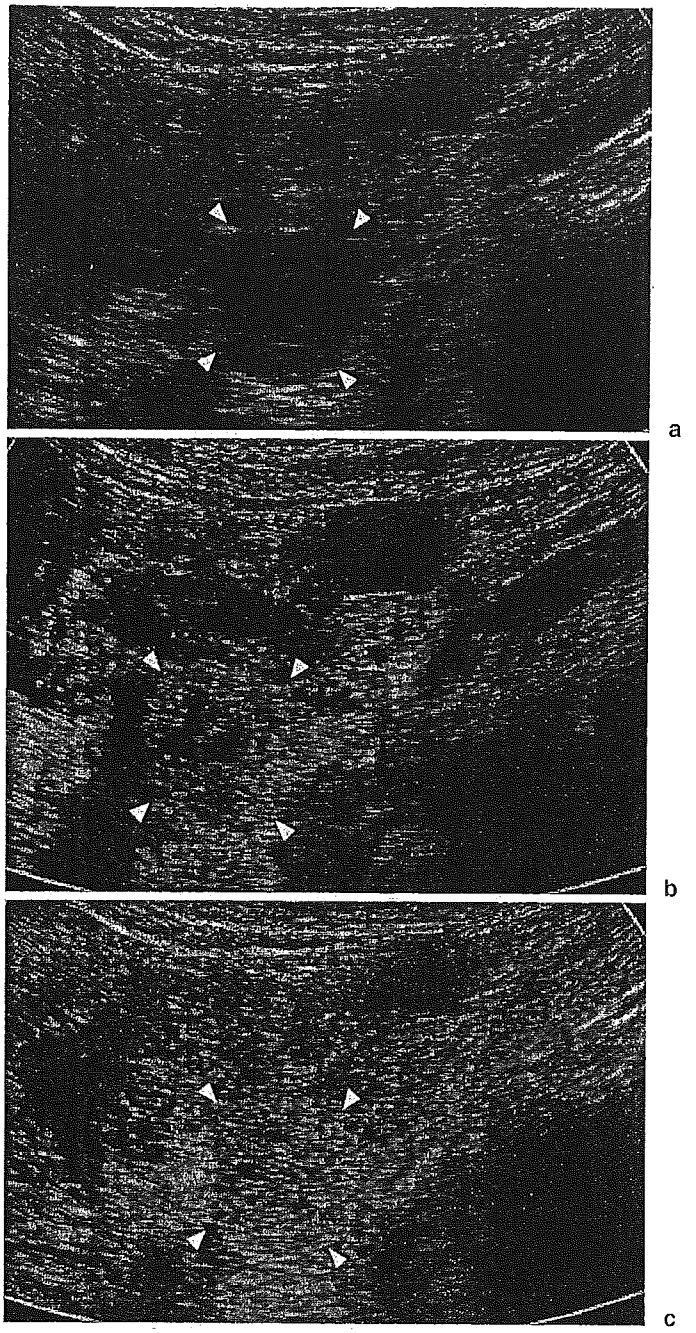

Fig. 4a–c. A case of pancreatic endocrine tumor. B-mode US showed a hypoechoic tumor **(a)**, and CE-US revealed a heterogeneous hypervascular pattern throughout the lesion both on the vascular image **(b)** and the perfusion image **(c)**. *Arrowheads* in **a** to **c** show the outline of the tumor

its arterial vessels. Levovist contrast imaging requires intermittent scanning, because the signals from the microbubbles are obtained when high-MI US destroys the microbubbles.[15–22] The ADI used in this study is a specific contrast mode for the high-MI contrast agent, Levovist. The ADI technique is similar to the Doppler mode, i.e., visualizing the signal coming from the